






## Quantum localization measures in phase space

D. Villaseñor <sup>1</sup>, S. Pilatowsky-Cameo <sup>1</sup>, M. A. Bastarrachea-Magnani <sup>2</sup>, S. Lerma-Hernández <sup>3</sup> and J. G. Hirsch <sup>1,\*</sup>

<sup>1</sup>*Instituto de Ciencias Nucleares, Universidad Nacional Autónoma de México, Apartado Postal 70-543, CP 04510 Ciudad de México, Mexico*

<sup>2</sup>*Departamento de Física, Universidad Autónoma Metropolitana-Iztapalapa, San Rafael Atlixco 186, CP 09340 Ciudad de México, Mexico*

<sup>3</sup>*Facultad de Física, Universidad Veracruzana, Circuito Aguirre Beltrán s/n, CP 91000 Xalapa, Veracruz, Mexico*



(Received 15 March 2021; accepted 23 April 2021; published 19 May 2021)

Measuring the degree of localization of quantum states in phase space is essential for the description of the dynamics and equilibration of quantum systems, but this topic is far from being understood. There is no unique way to measure localization, and individual measures can reflect different aspects of the same quantum state. Here we present a general scheme to define localization in measure spaces, which is based on what we call Rényi occupations, from which any measure of localization can be derived. We apply this scheme to the four-dimensional unbounded phase space of the interacting spin-boson Dicke model. In particular, we make a detailed comparison of two localization measures based on the Husimi function in the regime where the model is chaotic, namely, one that projects the Husimi function over the finite phase space of the spin and another that uses the Husimi function defined over classical energy shells. We elucidate the origin of their differences, showing that in unbounded spaces the definition of maximal delocalization requires a bounded reference subspace, with different selections leading to contextual answers.

DOI: [10.1103/PhysRevE.103.052214](https://doi.org/10.1103/PhysRevE.103.052214)

### I. INTRODUCTION

The term dynamical localization was coined to denote the quantum limitation of classical diffusion in the chaotic regime [1,2]. It was first observed in periodically kicked rotors and later it was also found in different systems, as the hydrogen atom in a monochromatic field and Rydberg atoms [3–5], as well as related to the Anderson localization present in one-dimensional disordered systems [6,7]. The phenomenon was also observed in conservative systems, such as the band-random-matrix model and quantum billiards [8–14], and more recent studies have focused its onset on many-body systems [15–17].

A usual way to measure delocalization is the exponential of entropy [18], which, under different names, is widely used throughout different areas of science. For example, in ecology, the diversity indices are used to count the number of species in a population [19]. In information science and linguistics, the perplexity quantifies how well a probabilistic model fits some data [20,21]. In physics, localization, understood as the exponential of entropy, is defined with respect to a given space. Using the phase space, one may draw a connection between the structures of classical dynamics and those of the quantum realm [22]. Quantum states may be represented in the phase space through the so-called Husimi function [23], and the exponential of the Wehrl entropy [24], which is the Shannon entropy of the Husimi function (or more generally Rényi-Wehrl entropies [25]), may be used to measure the localization of quantum states in that space.

In addition to a particular entropy and space, it may be necessary to choose specific subspaces or projections

of the Husimi function in order to talk about maximally delocalized states. When the measure space is unbounded (i.e., has infinite volume), one may find states that are arbitrarily delocalized and needs to choose a region of finite volume which serves as a benchmark. We will see that there is no universal way to do this, and a series of fundamental choices which have direct repercussions on the behavior of the localization measures must be made.

Recent studies [26,27] have used the exponential of the Rényi-Wehrl entropies to measure the localization of eigenstates in the phase space of the Dicke model. This model is a collective many-body system [28] initially introduced to explain the phenomenon of superradiance [29–32]. It describes a set of two-level atoms interacting collectively with a quantized radiation field and has been used extensively to study different phenomena, such as out-of-time-ordered correlators [33–35], quantum scarring [27,36–39], and nonequilibrium dynamics [32,40–44]. Some experimental realizations of this model involve superconducting circuits [45], cavity assisted Raman transitions [46,47], and trapped ions [48,49].

One purpose of this work is to identify the general mathematical framework from which any measure of localization can be derived. We will call these measures, which are exponentials of the Rényi entropies, Rényi volumes [50], and from them we will define the Rényi occupations, which are relative localization measures with respect to a finite reference volume. These general localization measures simplify to the usual generalized participation ratios for the case of a discrete set [51,52].

In this work two Rényi occupations based on Husimi functions are explored in detail in the unbounded phase space of the Dicke model. The first one is defined in the atomic phase space of the model, where the reference volume is defined in the Bloch sphere [26]. The second Rényi occupation

\*Corresponding author: [hirsch@nucleares.unam.mx](mailto:hirsch@nucleares.unam.mx)

is defined over classical energy shells, where the reference volume corresponds to the volume of the classical energy shell [27]. These two measures serve as examples for our general framework. We compare their behavior for eigenstates in the chaotic regime of the model and also their dynamical evolution for nonstationary states. Their dissimilar behaviors prove our assertion that there is no universal way to identify maximal delocalization in unbounded spaces.

The article is organized as follows. In Sec. II we expose a general method to define localization measures in bounded or unbounded spaces, discrete or continuous. In Sec. III we introduce the Dicke model and its classical limit. In Sec. IV we focus on localization measures in the four-dimensional phase space of the Dicke model, constructing two different Rényi occupations. In Sec. V we compare the behaviors of both Rényi occupations for different kinds of states, such as eigenstates, evolved coherent states, and mixed coherent states in time and in space. A summary and our conclusions are presented in Sec. VI.

## II. RÉNYI OCCUPATION IN GENERAL SPACES

Consider a space  $X$  with a measure  $\mathcal{V}$  that generates an integral  $\int_X d\mathcal{V}(\mathbf{x}) \bullet$ . This space may be discrete, in which case  $\mathcal{V}(\Omega) = |\Omega|$  ( $\Omega \subseteq X$ ) is the counting measure, whose integral is just a sum  $\int_X d\mathcal{V}(\mathbf{x}) \bullet = \sum_{\mathbf{x} \in X} \bullet$ . Regardless of the space, we will call  $\mathcal{V}(\Omega) = \int_\Omega d\mathcal{V}(\mathbf{x}) \in [0, \infty]$  the volume of  $\Omega \subseteq X$ . In  $X$ , we have normalized functions  $\varphi : X \rightarrow [0, \infty)$  [i.e.,  $\int_X d\mathcal{V}(\mathbf{x})\varphi(\mathbf{x}) = 1$ ], which we will call probability distributions.<sup>1</sup>

For any bounded measurable subset  $\Omega \subseteq X$ , the uniform probability distribution on  $\Omega$  is given by

$$\varphi_\Omega(\mathbf{x}) = \begin{cases} \frac{1}{\mathcal{V}(\Omega)} & \text{for } \mathbf{x} \in \Omega \\ 0 & \text{otherwise.} \end{cases} \quad (1)$$

We define the volume occupied by any probability distribution  $\varphi$  in  $X$ ,  $\mathcal{V}(X, \varphi)$ , by imposing the following properties.

(i) The volume occupied by a uniform probability is  $\mathcal{V}(X, \varphi_\Omega) = \mathcal{V}(\Omega)$ .

(ii) The volume is a homogeneous function of degree one under scaling of the measure  $\mathcal{V}(\Omega)$ , that is,

$$\mathcal{V}(X', \varphi') = k\mathcal{V}(X, \varphi), \quad (2)$$

where  $X' = X$  is the same space, but with volume element  $d\mathcal{V}' = kd\mathcal{V}$ , and  $\varphi'(\mathbf{x}) = \varphi(\mathbf{x})/k$ , with  $k > 0$ .

In Appendix A we show that these two conditions naturally lead to the expression

$$\mathcal{V}_\alpha(X, \varphi) = \left( \int_X d\mathcal{V}(\mathbf{x})\varphi(\mathbf{x})^\alpha \right)^{1/(1-\alpha)}, \quad (3)$$

which is the exponential of the Rényi entropy of order  $\alpha \geq 0$ ,  $H_\alpha(X, \varphi) = \ln[\int_X d\mathcal{V}(\mathbf{x})\varphi(\mathbf{x})^\alpha]/(1-\alpha)$  [18,53]. In the limit  $\alpha \rightarrow 1$  we get

$$\mathcal{V}_1(X, \varphi) = \exp\left(-\int_X d\mathcal{V}(\mathbf{x})\varphi(\mathbf{x})\ln\varphi(\mathbf{x})\right), \quad (4)$$

<sup>1</sup>If the space is discrete, then this probability density function is just the probability at each point  $\mathbf{x}_i \in X$ ,  $p_i = \varphi(\mathbf{x}_i)$ .

which is the exponential of the Shannon entropy  $H_1(X, \varphi)$  [54]. Due to this close relation with the Rényi entropies, we call  $\mathcal{V}_\alpha(X, \varphi)$  the Rényi volume of order  $\alpha$  [50,55].

The numbers  $\mathcal{V}_\alpha(X, \varphi)$  are always positive and grow as  $\varphi$  spreads more over  $X$ . For nonuniform distributions  $\varphi$  the Rényi volume is the volume of the effective region occupied by  $\varphi$  and its value depends strongly on  $\alpha$ . In any case, the Rényi volume of  $\varphi$  measures how delocalized  $\varphi$  is.

When the space  $X$  is bounded, that is,  $\mathcal{V}(X) < \infty$ , then  $\mathcal{V}_\alpha(X, \varphi) \leq \mathcal{V}(X)$  and the maximum Rényi volume  $\mathcal{V}_\alpha(X, \varphi) = \mathcal{V}(X)$  is attained by the uniform distribution over  $X$ . Moreover, if  $\alpha \neq 0$ , then  $\mathcal{V}_\alpha(X, \varphi) = \mathcal{V}(X)$  occurs only for the uniform distribution. Thus, for a bounded space  $X$ , we can define the Rényi occupation of order  $\alpha$  of  $\varphi$  in  $X$  through the ratio

$$\mathfrak{L}_\alpha(X, \varphi) = \frac{\mathcal{V}_\alpha(X, \varphi)}{\mathcal{V}(X)} \in (0, 1]. \quad (5)$$

In contrast, if  $X$  is unbounded, that is,  $\mathcal{V}(X) = \infty$ , we may find distributions  $\varphi$  that are arbitrarily delocalized. This can be seen by considering  $\Omega \subseteq X$  such that  $\mathcal{V}(\Omega)$  is arbitrarily large and taking the uniform distribution in  $\Omega$ . Thus, an unbounded space does not allow one to define a Rényi occupation directly. However, one may consider a smaller space  $\tilde{X}$  which is bounded and transform the probability distributions from  $X$  to  $\tilde{X}$ . A general method to perform this involves three fundamental steps.

(1) Choose a smaller space  $\tilde{X}$ , which may be some region of  $X$ .

(2) Choose a new volume element  $d\tilde{\mathcal{V}}$  for  $\tilde{X}$  such that the total volume is finite  $\tilde{\mathcal{V}}(\tilde{X}) < \infty$ .

(3) Choose a transformation of the probability distributions  $\varphi : X \rightarrow [0, \infty)$  into probability distributions  $\tilde{\varphi} : \tilde{X} \rightarrow [0, \infty)$ .

By following these three steps one may use Eq. (5) with  $\tilde{X}$  and  $\tilde{\varphi}$  to define a Rényi occupation  $\mathfrak{L}_\alpha(\tilde{X}, \tilde{\varphi})$ .

The fact that the exponential of an entropy provides a measure of localization [18] should not be surprising: Entropies are, by virtue of Boltzmann's entropy formula, the logarithm of the number of microstates that give rise to a certain macroscopic state. If we imagine  $X$  to be the space of possible microstates of a system and  $\varphi$  to be a distribution in  $X$ , then we can measure the level of delocalization of  $\varphi$  in  $X$  by just *counting* the number of microstates that compose it.

We close this section with a simple well-known example of the Rényi volume  $\mathcal{V}_\alpha$  found in discrete spaces. If  $\mathcal{B} = \{|\phi_k\rangle \mid k \in N \subseteq \mathbb{N}\}$  is a basis of some Hilbert space of dimension  $|N|$ , each state  $|\psi\rangle$  defines the probability function  $\varphi_\psi(|\phi_k\rangle) = |\langle\psi|\phi_k\rangle|^2$ . Setting  $\mathcal{V}$  to be the counting measure, Eq. (3) becomes

$$\mathcal{V}_\alpha(\mathcal{B}, \varphi_\psi) = \left( \sum_{k \in N} |\langle\psi|\phi_k\rangle|^{2\alpha} \right)^{1/(1-\alpha)}, \quad (6)$$

which corresponds to the generalized quantum participation ratios [51,52], where the case  $\alpha = 2$  reduces to

$$\mathcal{V}_2(\mathcal{B}, \varphi_\psi) = P_R = \left( \sum_{k \in N} |\langle\psi|\phi_k\rangle|^4 \right)^{-1}, \quad (7)$$

the standard quantum participation ratio, which has been used as a standard measure of the localization of state  $|\psi\rangle$  in the basis  $\mathcal{B}$  [56].

### III. DICKE MODEL

In the following sections, we will study the Rényi occupations in the Dicke model, which describes the interaction between a set of two-level systems and a single-mode confined electromagnetic field [28]. Setting  $\hbar = 1$ , the Hamiltonian of the model can be written as

$$\hat{H}_D = \omega \hat{a}^\dagger \hat{a} + \omega_0 \hat{J}_z + \frac{\gamma}{\sqrt{\mathcal{N}}} (\hat{J}_+ + \hat{J}_-) (\hat{a}^\dagger + \hat{a}), \quad (8)$$

where  $\omega$  is the radiation frequency of the electromagnetic field,  $\mathcal{N}$  is the number of two-level atoms with transition frequency  $\omega_0$ , and  $\gamma$  is the atom-field coupling strength. In addition,  $\hat{a}^\dagger$  ( $\hat{a}$ ) is the bosonic creation (annihilation) operator of the field mode,  $\hat{J}_{x,y,z} = \frac{1}{2} \sum_{k=1}^{\mathcal{N}} \hat{\sigma}_{x,y,z}^k$  are the collective pseudospin operators, and  $\hat{\sigma}_{x,y,z}$  are the Pauli matrices which satisfy the SU(2) algebra. In addition,  $\hat{J}_+$  ( $\hat{J}_-$ ) is the raising (lowering) collective pseudospin operator, defined by  $\hat{J}_\pm = \hat{J}_x \pm i\hat{J}_y$ .

The squared total pseudospin operator  $\hat{\mathbf{J}}^2 = \hat{J}_x^2 + \hat{J}_y^2 + \hat{J}_z^2$  has eigenvalues  $j(j+1)$ , which specify different invariant subspaces of the model. In this work, we use the maximum pseudospin value  $j = \mathcal{N}/2$ , which defines the totally symmetric atomic subspace that includes the ground state.

The Dicke model develops a quantum phase transition when its coupling strength reaches the critical value  $\gamma_c = \sqrt{\omega\omega_0}/2$  [29,30,57,58]. At that point the system goes from a normal phase ( $\gamma < \gamma_c$ ) to a superradiant phase ( $\gamma > \gamma_c$ ).

The model displays regular and chaotic behavior, depending on the Hamiltonian parameters and excitation energies [59]. Here we consider a coupling in the superradiant phase,  $\gamma = 2\gamma_c = 1$ , where the system is in the strong-coupling hard-chaos regime. Also, we choose the resonant frequency case  $\omega = \omega_0 = 1$  and use energies rescaled to the system size  $j = 30$ . The diagonalization techniques for the Dicke Hamiltonian are fully explained in Appendix B.

#### Classical limit of the Dicke model

A classical Dicke Hamiltonian is obtained by taking the expectation value of the quantum Hamiltonian  $\hat{H}_D$  under the tensor product of bosonic Glauber and atomic Bloch coherent states  $|\mathbf{x}\rangle = |q, p\rangle \otimes |Q, P\rangle$  [36,44,59–63] and dividing it by the system size  $j$ ,

$$h_{\text{cl}}(\mathbf{x}) = \frac{\langle \mathbf{x} | \hat{H}_D | \mathbf{x} \rangle}{j} = \frac{\omega}{2} (q^2 + p^2) + \frac{\omega_0}{2} Z^2 + 2\gamma q Q \sqrt{1 - \frac{Z^2}{4}} - \omega_0, \quad (9)$$

where  $Z^2 = Q^2 + P^2$ . The bosonic Glauber and atomic Bloch coherent states are, respectively,

$$|q, p\rangle = e^{-(j/4)(q^2+p^2)} e^{[\sqrt{j/2}(q+ip)]\hat{a}^\dagger} |0\rangle, \\ |Q, P\rangle = \left(1 - \frac{Z^2}{4}\right)^j e^{[(Q+iP)/\sqrt{4-Z^2}]\hat{J}_+} |j, -j\rangle, \quad (10)$$

where  $|0\rangle$  is the photon vacuum and  $|j, -j\rangle$  is the state with all the atoms in the ground state.

The classical Hamiltonian  $h_{\text{cl}}(\mathbf{x})$  has a four-dimensional phase space  $\mathcal{M}$  in the coordinates  $\mathbf{x} = (q, p, Q, P)$ . The rescaled classical energy  $\epsilon = E/j$  that corresponds to  $h_{\text{cl}}$  defines an effective Planck constant  $\hbar_{\text{eff}} = 1/j$  [64].

### IV. RÉNYI OCCUPATIONS IN THE PHASE SPACE OF THE DICKE MODEL

#### A. Husimi function

The Husimi function is a quasiprobability distribution function [23,65] defined as the expectation value of the density matrix  $\hat{\rho}$  of an arbitrary state in the overcomplete coherent-state basis  $\{|\mathbf{x}\rangle \mid \mathbf{x} = (q, p, Q, P)\}$ ,

$$\mathcal{Q}_{\hat{\rho}}(\mathbf{x}) = \langle \mathbf{x} | \hat{\rho} | \mathbf{x} \rangle. \quad (11)$$

The Husimi function is a Wigner function [66] smoothed by a Gaussian weight and it is used to visualize how a state  $\hat{\rho}$  is distributed in the phase space. In contrast to the Wigner function, the Husimi function is everywhere non-negative. When  $\hat{\rho} = |\psi\rangle\langle\psi|$  is a pure state, it can be written as

$$\mathcal{Q}_{\psi}(\mathbf{x}) = |\langle \psi | \mathbf{x} \rangle|^2. \quad (12)$$

#### B. Rényi volume in the phase space

As the first step to study the Rényi occupations, we will calculate the Rényi volume for the phase space of the Dicke model  $\mathcal{M}$  with the canonical volume element  $d\mathcal{V}(\mathbf{x}) = dq dp dQ dP$ , which we will denote by  $d\mathbf{x}$ . Each state  $\hat{\rho}$  generates a probability distribution  $\varphi_{\hat{\rho}}(\mathbf{x})$  via the Husimi function [see Eq. (11)]

$$\varphi_{\hat{\rho}}(\mathbf{x}) = \frac{1}{C} \mathcal{Q}_{\hat{\rho}}(\mathbf{x}), \quad (13)$$

where  $C = \int_{\mathcal{M}} d\mathbf{x} \mathcal{Q}_{\hat{\rho}}(\mathbf{x}) = [2\pi/j] \times [4\pi/(2j+1)]$  ensures normalization.

By using Eqs. (3) and (4) with  $X = \mathcal{M}$  and  $\varphi = \varphi_{\hat{\rho}}$ , we get

$$\mathcal{V}_1(\mathcal{M}, \hat{\rho}) = C \exp\left(-\frac{1}{C} \int_{\mathcal{M}} d\mathbf{x} \mathcal{Q}_{\hat{\rho}}(\mathbf{x}) \ln \mathcal{Q}_{\hat{\rho}}(\mathbf{x})\right) \quad (14)$$

and

$$\mathcal{V}_{\alpha}(\mathcal{M}, \hat{\rho}) = C^{\alpha/(\alpha-1)} \left( \int_{\mathcal{M}} d\mathbf{x} \mathcal{Q}_{\hat{\rho}}^{\alpha}(\mathbf{x}) \right)^{1/(1-\alpha)} \quad (15)$$

for  $\alpha \geq 0$ . Equation (14) is the exponential of the Wehrl entropy [24]. These types of measures have been studied in the SU(2) two-dimensional phase space in Refs. [25,67].

By definition,  $\mathcal{V}_{\alpha}(\mathcal{M}, \hat{\rho}) > 0$ , but the quantum uncertainty principle actually provides a positive lower bound on the localization of a quantum state in the phase space. Namely, if  $\alpha \gg \hbar_{\text{eff}}^2$ ,

$$\mathcal{V}_{\alpha}(\mathcal{M}, \hat{\rho}) \geq (2\pi \hbar_{\text{eff}})^2 \alpha^{2/(\alpha-1)}, \quad (16)$$

where  $\hbar_{\text{eff}} = 1/j$  (see Appendix C for details). Nevertheless, there is no upper bound on the Rényi volume occupied by a quantum state because the phase space of the Dicke model is unbounded,  $\mathcal{V}(\mathcal{M}) = \int_{\mathcal{M}} d\mathbf{x} = \infty$ . Thus, we can find arbitrarily delocalized states.

TABLE I. Fundamental steps made in the construction of the Rényi occupations of order  $\alpha$  (see Sec. II), defined in the atomic subspace of the Dicke model  $\mathcal{L}_\alpha(\mathcal{A}, \hat{\rho})$  and over classical energy shells  $\mathcal{L}_\alpha(\epsilon, \hat{\rho})$ .

Rényi occupation	Step 1	Step 2		Step 3
	Subspace $\tilde{X}$	Volume element $d\mathcal{V}$	Volume $\mathcal{V}(\tilde{X})$	Distribution $\varphi_{\tilde{X}, \hat{\rho}}$
$\mathcal{L}_\alpha(\mathcal{A}, \hat{\rho})$	$\mathcal{A}$	$dQdP$	$4\pi$	$\frac{\tilde{Q}_{\hat{\rho}}(Q, P)}{C}$
$\mathcal{L}_\alpha(\epsilon, \hat{\rho})$	$\mathcal{M}_\epsilon$	$\delta(h_{\text{cl}}(\mathbf{x}) - \epsilon)d\mathbf{x}$	$4\pi^2\nu(\epsilon)$	$\frac{\mathcal{Q}_{\hat{\rho}}(\mathbf{x})}{C_\epsilon}$

In order to define a Rényi occupation in the phase space of the Dicke model  $\mathcal{M}$ , we may apply the measure outlined in Sec. II for unbounded spaces. This is done by restricting the measure to bounded regions of  $\mathcal{M}$ . We will focus on two different Rényi occupations for  $\mathcal{M}$ , which use the atomic subspace and the classical energy shells as bounded regions.

### C. Rényi occupation in the atomic subspace

A Rényi occupation using the atomic subspace of the Dicke model was originally studied in Ref. [26]. The complete phase space of the Dicke model consists of a bounded (atomic) subspace and an unbounded (bosonic) subspace. In some sense, selecting the atomic subspace as the finite-volume reference region seems to be the most natural choice to construct a Rényi occupation. This can be done by following steps 1–3 of Sec. II (see Table I for a summary of the steps). First, we choose the atomic subspace

$$\mathcal{A} = \{(Q, P) \mid Q^2 + P^2 \leq 4\} \quad (\text{step 1}), \quad (17)$$

with the canonical area element

$$d\mathcal{V}(Q, P) = dQdP \quad (\text{step 2}). \quad (18)$$

The subspace  $\mathcal{A}$  is bounded with respect to  $\mathcal{V}$ ,

$$\mathcal{V}(\mathcal{A}) = \int_{\mathcal{A}} dQdP = 4\pi. \quad (19)$$

For each state  $\hat{\rho}$  consider the probability distribution given by the projection of the Husimi function into  $\mathcal{A}$ ,

$$\varphi_{\mathcal{A}, \hat{\rho}}(Q, P) = \frac{1}{C} \tilde{Q}_{\hat{\rho}}(Q, P) \quad (\text{step 3}), \quad (20)$$

where

$$\tilde{Q}_{\hat{\rho}}(Q, P) = \iint dq dp \mathcal{Q}_{\hat{\rho}}(q, p; Q, P) \quad (21)$$

and  $C = [2\pi/j] \times [4\pi/(2j+1)]$  ensures normalization. Using Eq. (5) with  $X = \mathcal{A}$ ,  $\varphi = \varphi_{\mathcal{A}, \hat{\rho}}$ , and  $\mathcal{V}(\mathcal{A}) = 4\pi$ , we obtain the Rényi occupations on the atomic

subspace

$$\begin{aligned} \mathcal{L}_1(\mathcal{A}, \hat{\rho}) &= \frac{C}{4\pi} \exp\left(-\frac{1}{C} \int_{\mathcal{A}} dQdP \tilde{Q}_{\hat{\rho}}(Q, P) \ln \tilde{Q}_{\hat{\rho}}(Q, P)\right) \quad (22) \end{aligned}$$

and

$$\mathcal{L}_\alpha(\mathcal{A}, \hat{\rho}) = \frac{C^{\alpha/(\alpha-1)}}{4\pi} \left( \int_{\mathcal{A}} dQdP \tilde{Q}_{\hat{\rho}}^\alpha(Q, P) \right)^{1/(1-\alpha)}. \quad (23)$$

The Rényi occupation of order  $\alpha = 2$ , which we will henceforth focus on, reads

$$\mathcal{L}_2(\mathcal{A}, \hat{\rho}) = \frac{C^2}{4\pi} \left( \int_{\mathcal{A}} dQdP \tilde{Q}_{\hat{\rho}}^2(Q, P) \right)^{-1}, \quad (24)$$

which along with that of order  $\alpha = 1$ , was studied in detail in Ref. [26] for eigenstates  $\hat{\rho} = |E_k\rangle\langle E_k|$  of the Dicke model. In that work, these Rényi occupations were also multiplied by an additional factor which equals the percentage of  $\mathcal{A}$  that is covered by classical chaotic trajectories, and a linear relation between  $\mathcal{L}_1(\mathcal{A}, \hat{\rho})$  and  $\mathcal{L}_2(\mathcal{A}, \hat{\rho})$  was found for some of the eigenstates in the chaotic regime.

### D. Rényi occupation over classical energy shells

Because of the energy conservation, the temporal evolution of any initial state under a time-independent Hamiltonian will maintain the same average energy. States with a well-defined energy center will remain close to the corresponding classical energy shell in the phase space.

This motivates us to define another Rényi occupation by using the bounded classical energy shells as reference subspaces, as it was done in Ref. [27]. This can be achieved by applying steps 1–3 of Sec. II as follows (see Table I for a summary).

Consider the classical energy shell at energy  $\epsilon$ ,

$$\mathcal{M}_\epsilon = \{\mathbf{x} = (q, p; Q, P) \mid h_{\text{cl}}(\mathbf{x}) = \epsilon\} \quad (\text{step 1}), \quad (25)$$

with the surface volume element

$$d\mathcal{V}(\mathbf{x}) = \delta(h_{\text{cl}}(\mathbf{x}) - \epsilon)d\mathbf{x} \quad (\text{step 2}), \quad (26)$$

which we will denote by  $ds$ . The subspace  $\mathcal{M}_\epsilon$  is bounded with respect to  $\mathcal{V}$ . In fact, the finite value  $\mathcal{V}(\mathcal{M}_\epsilon)$  can be calculated through the quantity

$$\nu(\epsilon) = \frac{1}{4\pi^2} \mathcal{V}(\mathcal{M}_\epsilon) = \frac{1}{4\pi^2} \int_{\mathcal{M}_\epsilon} ds, \quad (27)$$

which is the lowest-order semiclassical approximation for the quantum density of states obtained through the Gutzwiller trace formula [68,69]. See Ref. [61] for a detailed analytical expression of this semiclassical density of states  $\nu(\epsilon)$ .

For each state  $\hat{\rho}$ , consider the probability distribution given by the restriction of the Husimi function to  $\mathcal{M}_\epsilon$ ,

$$\varphi_{\epsilon, \hat{\rho}}(\mathbf{x}) = \frac{1}{C_\epsilon} \mathcal{Q}_{\hat{\rho}}(\mathbf{x}) \quad (\text{step 3}), \quad (28)$$

where  $C_\epsilon = \int_{\mathcal{M}_\epsilon} ds \mathcal{Q}_{\hat{\rho}}(\mathbf{x})$  ensures normalization. Using Eq. (5) with  $X = \mathcal{M}_\epsilon$ ,  $\varphi = \varphi_{\epsilon, \hat{\rho}}$ , and  $\mathcal{V}(\mathcal{M}_\epsilon) = 4\pi^2\nu(\epsilon)$ , we

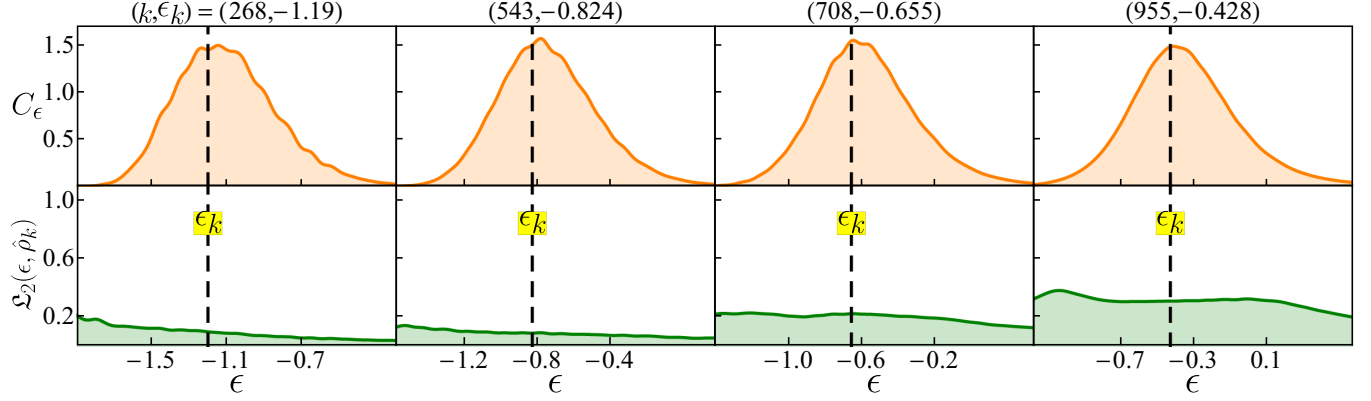


FIG. 1. Shown on top is the energy profile  $C_\epsilon$  of the Husimi function over the classical energy shell at  $\epsilon$  for selected eigenstates  $\hat{\rho}_k$  with  $k = 268, 543, 708, 955$  in the energy region  $\epsilon_k \in (-1.2, -0.43)$ . Shown on the bottom is the Rényi occupation  $\mathcal{L}_2(\epsilon, \hat{\rho}_k)$  [see Eq. (31)] as a function of the energy  $\epsilon$  for the same selected eigenstates. In both the top and bottom panels, the vertical dashed black lines indicate the eigenenergies  $\epsilon_k$  of the corresponding eigenstates  $\hat{\rho}_k$ . The system size is  $j = 30$ .

obtain the set of Rényi occupations over the energy shell at  $\epsilon$ ,

$$\mathcal{L}_1(\epsilon, \hat{\rho}) = \frac{C_\epsilon}{4\pi^2\nu(\epsilon)} \exp\left(-\frac{1}{C_\epsilon} \int_{\mathcal{M}_\epsilon} ds \mathcal{Q}_{\hat{\rho}}(x) \ln \mathcal{Q}_{\hat{\rho}}(x)\right) \quad (29)$$

and

$$\mathcal{L}_\alpha(\epsilon, \hat{\rho}) = \frac{C_\epsilon^{\alpha/(\alpha-1)}}{4\pi^2\nu(\epsilon)} \left( \int_{\mathcal{M}_\epsilon} ds \mathcal{Q}_{\hat{\rho}}^\alpha(x) \right)^{1/(1-\alpha)}. \quad (30)$$

The Rényi occupation of order  $\alpha = 2$ ,

$$\mathcal{L}_2(\epsilon, \hat{\rho}) = \frac{C_\epsilon^2}{4\pi^2\nu(\epsilon)} \left( \int_{\mathcal{M}_\epsilon} ds \mathcal{Q}_{\hat{\rho}}^2(x) \right)^{-1}, \quad (31)$$

was used in Ref. [27] to measure localization of eigenstates and temporally averaged evolved states in the Dicke model in relation to the phenomenon of quantum scarring. It was also used as a measure of quantum ergodicity. Henceforth, we will focus on this specific case  $\alpha = 2$  and leave a detailed study of the dependence on the order  $\alpha$  and its relation to multifractality [51,70–76] for future work.

Given a quantum state  $\hat{\rho}$  with mean energy  $\epsilon_{\hat{\rho}} = \text{tr}(\hat{\rho}\hat{H}_D)$ , we may measure its localization in the phase-space energy shell at any energy  $\epsilon$  through  $\mathcal{L}_2(\epsilon, \hat{\rho})$ . Nevertheless, for eigenstates  $\hat{\rho}_k = |E_k\rangle\langle E_k|$ , a natural choice is  $\epsilon = \epsilon_{\hat{\rho}_k} = \epsilon_k$ . Moreover,  $\mathcal{L}_2(\epsilon, \hat{\rho}_k)$  remains almost constant for the energies around  $\epsilon_k = E_k/j$  that are significantly populated by the state  $\hat{\rho}_k$ . The top panels of Fig. 1 show the energy profiles  $C_\epsilon = \int_{\mathcal{M}_\epsilon} ds \mathcal{Q}_{\hat{\rho}}(x)$  of four selected eigenstates, one ( $k = 268$ ) located in a mixed energy region where regularity and chaos coexist and three ( $k = 543, 708, 955$ ) located in the fully chaotic-energy regime. These energy profiles show that the Husimi functions of the respective eigenstates are concentrated in energy shells with relevant values in an interval around  $\epsilon \sim \epsilon_k$ , while the bottom panels show that  $\mathcal{L}_2(\epsilon, \hat{\rho}_k)$  is almost constant in the region of significant population. It is worth mentioning that we have found that the Rényi occupation  $\mathcal{L}_2(\epsilon, \hat{\rho}_k)$  can be more sensitive to  $\epsilon$  at low energies due to the regularity of the dynamics and because at energies close to the ground-state energy  $\epsilon_{GS} = -2.125$ , the classical energy shells are very small and their size increases rapidly as energy

does. Nevertheless, for the energy regime studied in this work, these effects are negligible.

## V. PROPERTIES OF RÉNYI OCCUPATIONS IN THE PHASE SPACE OF THE DICKE MODEL

The Rényi occupations that we presented in the preceding section have been used to measure the localization of the eigenstates in the chaotic regime [26,27]. The statistical properties of the localization of eigenstates can be tied to the chaoticity of quantum systems. For example, a relatively low value of Rényi occupation can be a signal of quantum scarring. The localization of the eigenstates also has an impact on the evolution of nonstationary states, such as coherent states. Thus, studying the dynamical evolution of the localization of coherent states also provides very useful information about the dynamical properties of the system.

In this section we compare the Rényi occupations of the Husimi projection over the atomic subspace  $\mathcal{L}_2(\mathcal{A}, \hat{\rho})$  [see Eq. (24)] and over classical energy shells  $\mathcal{L}_2(\epsilon, \hat{\rho})$  [see Eq. (31)], for eigenstates, time-evolved coherent states, and coherent states mixed in phase space.

### A. Localization of eigenstates

For a set of 501 eigenstates of the Dicke model  $\hat{\rho}_k = |E_k\rangle\langle E_k|$  with  $k \in [3121, 3621]$ , located in the chaotic-energy region  $\epsilon_k \in (1, 1.274)$ , we compute both Rényi occupations  $\mathcal{L}_2(\mathcal{A}, \hat{\rho}_k)$  and  $\mathcal{L}_2(\epsilon_k, \hat{\rho}_k)$ . The distributions for both occupations are shown in Fig. 2. In this figure we see that the occupation  $\mathcal{L}_2(\mathcal{A}, \hat{\rho}_k)$  clusters around the mean value  $\mathcal{L}_2 \sim 0.9$ , which means that the Husimi projections of all eigenstates in this chaotic region are almost completely delocalized in the atomic Bloch sphere  $\mathcal{A}$ . On the other hand, the occupation  $\mathcal{L}_2(\epsilon_k, \hat{\rho}_k)$  clusters around a mean value  $\mathcal{L}_2 \sim 0.4$ , indicating that all eigenstates occupy less than half of the classical energy shell at  $\epsilon_k$ .

The striking differences between both Rényi occupations  $\mathcal{L}_2(\mathcal{A}, \hat{\rho}_k)$  and  $\mathcal{L}_2(\epsilon_k, \hat{\rho}_k)$  indicate that they gauge different aspects of the same eigenstates and show that one has to be cautious in interpreting the values provided by different localization measures. Below we provide several numerical tests

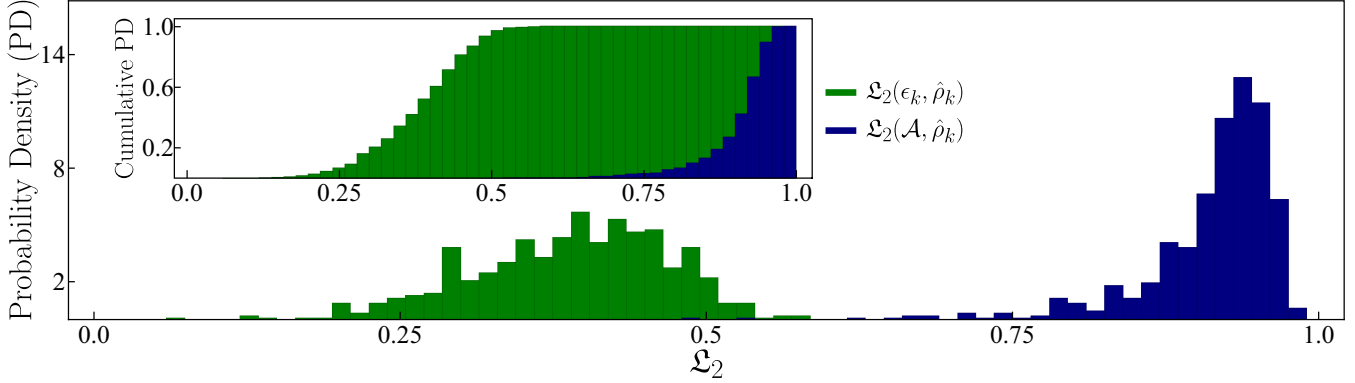


FIG. 2. Statistical distributions of the Rényi occupations  $\mathcal{L}_2(\mathcal{A}, \hat{\rho}_k)$  (blue bars) and  $\mathcal{L}_2(\epsilon_k, \hat{\rho}_k)$  (green bars) [see Eqs. (24) and (31)] for a set of 501 eigenstates  $\hat{\rho}_k$  with  $k \in [3121, 3621]$ , located in the chaotic-energy region  $\epsilon_k \in (1.0, 1.274)$ . The inset shows their corresponding cumulative distributions. The system size is  $j = 30$ .

allowing us to clarify the origin of the differences obtained for both Rényi occupations.

### B. Localization of evolved coherent states

Consider initial Glauber-Bloch coherent states  $\hat{\rho}_x = |\mathbf{x}\rangle\langle\mathbf{x}|$ , with coordinates  $\mathbf{x} = (q_0, p_0; Q_0, P_0)$  and mean energy  $\epsilon_x = h_{\text{cl}}(\mathbf{x})$ , which are highly localized in the phase space. The time evolution of  $\hat{\rho}_x$  is given by

$$\hat{\rho}_x(t) = \hat{U}(t)|\mathbf{x}\rangle\langle\mathbf{x}|\hat{U}^\dagger(t), \quad (32)$$

where  $\hat{U}^\dagger(t) = e^{-i\hat{H}t}$ . We study how the initial state  $\hat{\rho}_x$  delocalizes as it evolves in time by considering the Rényi occupations  $\mathcal{L}_2(\mathcal{A}, \hat{\rho}_x(t))$  and  $\mathcal{L}_2(\epsilon_x, \hat{\rho}_x(t))$ . In Fig. 3(a) we see that  $\mathcal{L}_2(\mathcal{A}, \hat{\rho}_x(t))$  quickly saturates to 1, indicating that the evolved coherent state becomes fully delocalized in the atomic subspace  $\mathcal{A}$ . On the other hand, the measure  $\mathcal{L}_2(\epsilon_x, \hat{\rho}_x(t))$  saturates to a value of  $\frac{1}{2}$ , indicating that an evolved coherent state never delocalizes completely, being able to cover at most half of the energy shell at large times. This is in accord with the results of Ref. [27], where it was found that  $\mathcal{L}_2 \lesssim \frac{1}{2}$  for any pure state, and complete delocalization within a classical energy shell can only be reached when temporal averages are performed.

For this reason, in Fig. 3(b) we plot the values of the Rényi occupations  $\mathcal{L}_2(\mathcal{A}, \bar{\rho}_x(T))$  and  $\mathcal{L}_2(\epsilon_x, \bar{\rho}_x(T))$  for the time-averaged state

$$\bar{\rho}_x(T) = \frac{1}{T} \int_0^T dt \hat{\rho}_x(t). \quad (33)$$

We see that the Rényi occupation  $\mathcal{L}_2(\epsilon_x, \bar{\rho}_x(T))$  saturates to 1 at a time larger than the saturation time of the instantaneous localization of the evolved state  $\hat{\rho}(t)$ . In contrast, for  $\mathcal{L}_2(\mathcal{A}, \bar{\rho}_x(T))$ , a dip appears around  $T = 2$ , which is absent in  $\mathcal{L}_2(\epsilon_x, \bar{\rho}_x(T))$ . This is explained by the atomic and bosonic projections, shown in the top and middle panels of Fig. 3(b), respectively. At  $T = 1$ , the atomic projection of  $\bar{\rho}_x(T)$  looks like a closed orbit, which starts to retrace itself at  $T = 2$ , producing an apparent increased localization which is clearly visible as a bright area in the third atomic projection. However, this apparently closed orbit is not closed in the complete phase space. One sees from the bosonic projection in  $T = 2$

that, in fact, the state is not revisiting the same region but delocalizing over the bosonic variables. This effect is absent in  $\mathcal{L}_2(\epsilon_x, \bar{\rho}_x(T))$ , where no projection is performed. In that case, the temporal average only smooths out the quantum fluctuations, allowing for a less abrupt route to saturation with a slightly larger saturation time.

### C. Separation of coherent states in the atomic and bosonic planes

To further study the different behaviors of the Rényi occupations  $\mathcal{L}_2(\mathcal{A}, \hat{\rho})$  and  $\mathcal{L}_2(\epsilon, \hat{\rho})$ , we investigate what happens when we consider a mixed state formed by two coherent states whose centroids are gradually separated in different directions. By doing this, we want to investigate how sensitive the measures are to a gradual delocalization in both the atomic ( $Q, P$ ) and bosonic ( $q, p$ ) coordinate planes. We consider the mixed state of a pair of coherent states

$$\hat{\rho}_M(D) = \frac{1}{2}(\hat{\rho}_x + \hat{\rho}_y), \quad (34)$$

where the state  $\hat{\rho}_x = |\mathbf{x}\rangle\langle\mathbf{x}|$  remains fixed at position  $\mathbf{x}$  while the position  $\mathbf{y}$  of state  $\hat{\rho}_y = |\mathbf{y}\rangle\langle\mathbf{y}|$  is varied and their phase-space distance given by

$$D = \sqrt{(q_x - q_y)^2 + (p_x - p_y)^2 + \Theta^2}, \quad (35)$$

where

$$\cos \Theta = \cos \theta_x \cos \theta_y + \cos(\phi_x - \phi_y) \sin \theta_x \sin \theta_y, \quad (36)$$

with  $\cos \theta = 1 - (Q^2 + P^2)/2$  and  $\tan \phi = -P/Q$ . The coordinates of  $\mathbf{y}$  start with both states at the same position  $D = 0$  and are changed such that the mean energy  $\epsilon_M$  and energy width of  $|\mathbf{y}\rangle$  remain constant. These conditions ensure that the changes in the occupation measures come exclusively from the separation of the coherent state and not from changes in the properties of the coherent states  $|\mathbf{y}\rangle$ .

First we separate the states in the atomic plane ( $Q, P$ ) by letting  $p_y = p_x$  be constant and changing  $q_y$  slightly to maintain the mean energy of  $|\mathbf{y}\rangle$  constant. Figure 4(a) shows the projection of  $\hat{\rho}_M(D)$  in both the atomic and bosonic coordinate planes (top square panels) and the values of the Rényi occupations as a function of the separation  $D$

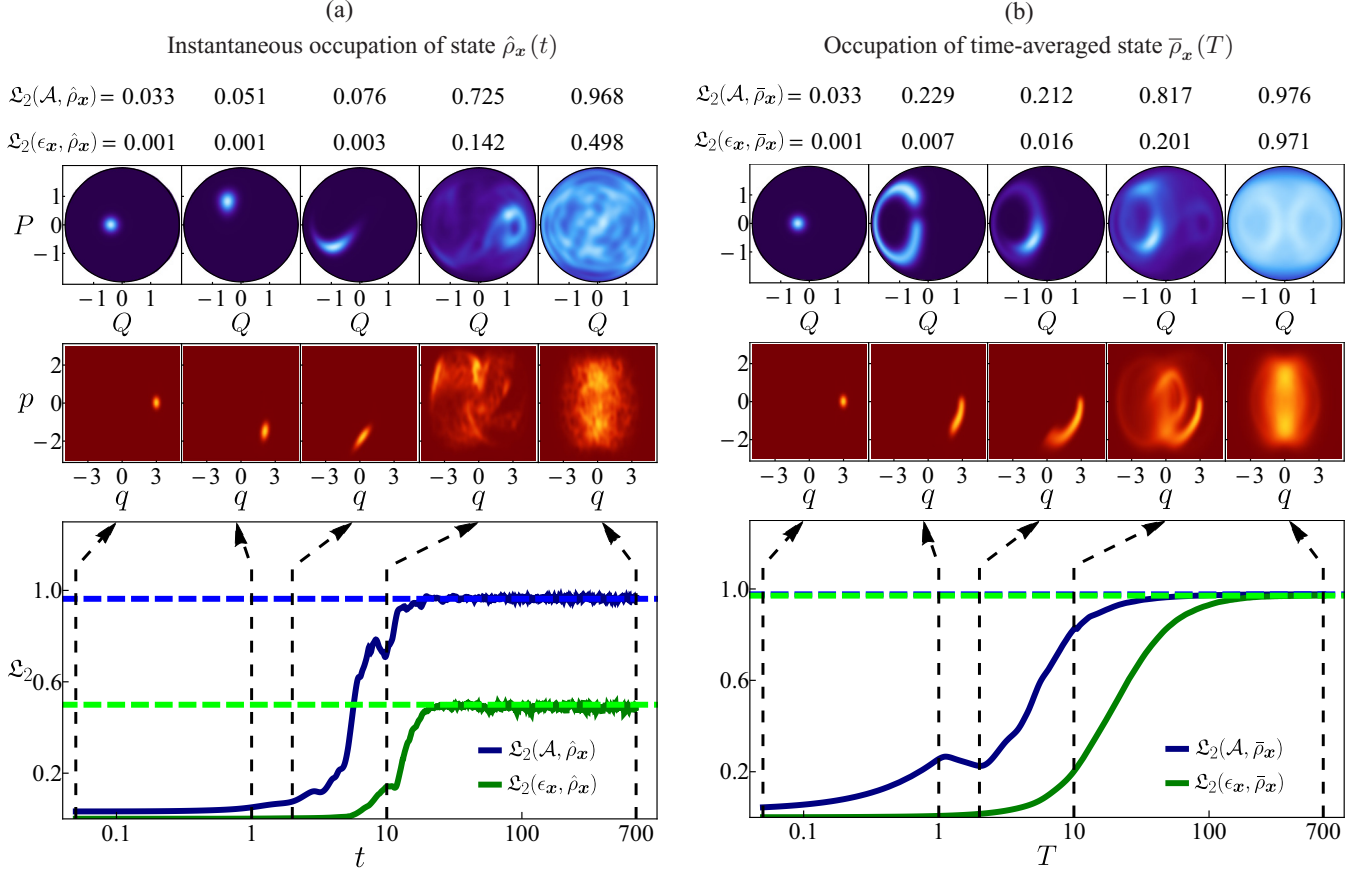


FIG. 3. The top square panels show the Husimi function projected in the atomic coordinate plane  $(Q, P)$  at different times  $t$  and  $T$  for both (a) the pure  $\hat{\rho}_x(t)$  state and (b) the time-mixed  $\bar{\rho}_x(T)$  coherent state [see Eqs. (32) and (33)]. The bottom rectangular panels show the Rényi occupations  $\mathcal{L}_2(\mathcal{A}, \hat{\rho}_x(t))$  [ $\mathcal{L}_2(\mathcal{A}, \bar{\rho}_x(T))$ ] (solid blue curve) and  $\mathcal{L}_2(\epsilon_x, \hat{\rho}_x(t))$  [ $\mathcal{L}_2(\epsilon_x, \bar{\rho}_x(T))$ ] (solid green curve) [see Eqs. (24) and (31)] for (a) a pure initial coherent state  $\hat{\rho}_x(t)$  and (b) the time-mixed coherent state  $\bar{\rho}_x(T)$  in the chaotic-energy region  $\epsilon_x = 1$ . The selected initial coherent state  $\hat{\rho}_x$  is defined by the phase-space coordinates  $\mathbf{x} = (2.894, 0; -0.4, 0)$  with energy width  $\sigma_x = 0.693$  (units of  $\epsilon$ ). Horizontal dashed green and blue lines indicate the asymptotic value of each measure in both panels. Vertical dashed black lines indicate the value of  $t$  and  $T$  where the Husimi projections are shown. The system size is  $j = 30$ .

(bottom rectangular panel). The Rényi occupations are divided by their values at  $D = 0$ ,  $\mathcal{L}_2(\mathcal{A}, \hat{\rho}_M)/\mathcal{L}_2(\mathcal{A}, \hat{\rho}_M(0))$  and  $\mathcal{L}_2(\epsilon_M, \hat{\rho}_M)/\mathcal{L}_2(\epsilon_M, \hat{\rho}_M(0))$ , allowing us to compare their relative growth. We see that in this case both Rényi occupations behaves similarly, increasing to twice their original value.

Now we separate the states in the bosonic plane  $(q, p)$ , letting  $Q_y = Q_x$  and  $P_y = P_x$  remain constant, as shown in Fig. 4(b). Contrary to the previous case, the results show remarkable differences between  $\mathcal{L}_2(\mathcal{A}, \hat{\rho}_M)$  and  $\mathcal{L}_2(\epsilon_M, \hat{\rho}_M)$ . While the Rényi occupation  $\mathcal{L}_2(\epsilon_M, \hat{\rho}_M)$  behaves as in the previous case, doubling its value,  $\mathcal{L}_2(\mathcal{A}, \hat{\rho}_M)$  remains constant. We see that the Rényi occupation  $\mathcal{L}_2(\mathcal{A}, \hat{\rho}_M)$  is not sensitive to delocalization in the bosonic plane, which is a consequence of the partial integration over the bosonic variables  $(q, p)$  in Eq. (21) that erases the information about delocalization in the bosonic plane.

#### D. Saturation of atomic plane

We now focus on how  $\mathcal{L}_2(\mathcal{A}, \hat{\rho})$  and  $\mathcal{L}_2(\epsilon, \hat{\rho})$  respond to a decreasing localization in the atomic plane  $(Q, P)$  but

letting the state be well localized in the bosonic one  $(q, p)$ . We consider a mixed state comprised of  $n$  coherent states

$$\hat{\rho}_M(n) = \frac{1}{n} \sum_{i=1}^n |\mathbf{x}_i\rangle\langle\mathbf{x}_i|, \quad (37)$$

whose centroids  $\mathbf{x}_i$  are homogeneously distributed over an increasing area of the Bloch sphere, as shown in the top panels of Fig. 5, but have the same classical energy  $\epsilon_M = h_{cl}(\mathbf{x}_i)$ .

We computed  $\mathcal{L}_2(\mathcal{A}, \hat{\rho}_M)$  and  $\mathcal{L}_2(\epsilon_M, \hat{\rho}_M)$  as we increased the Bloch sphere area occupied by the mixed state by increasing  $n$  and plotted the result in Fig. 5. Note that the Rényi occupation  $\mathcal{L}_2(\mathcal{A}, \hat{\rho}_M)$  saturates completely to unity when we fill completely the Bloch sphere, even if the states are highly localized in the bosonic plane. On the other hand, the Rényi occupation  $\mathcal{L}_2(\epsilon_M, \hat{\rho}_M)$  is sensitive to the localization of the mixed state in the bosonic plane and consequently it reaches a very small value of  $\mathcal{L}_2 \sim 0.07$ , indicating that the state  $\hat{\rho}_M$  only covers approximately 7% of the phase-space volume of the energy shell at  $\epsilon_M$ . This is understandable when we see the Husimi projections. Even when the atomic projection fills completely the Bloch sphere, the bosonic projections show

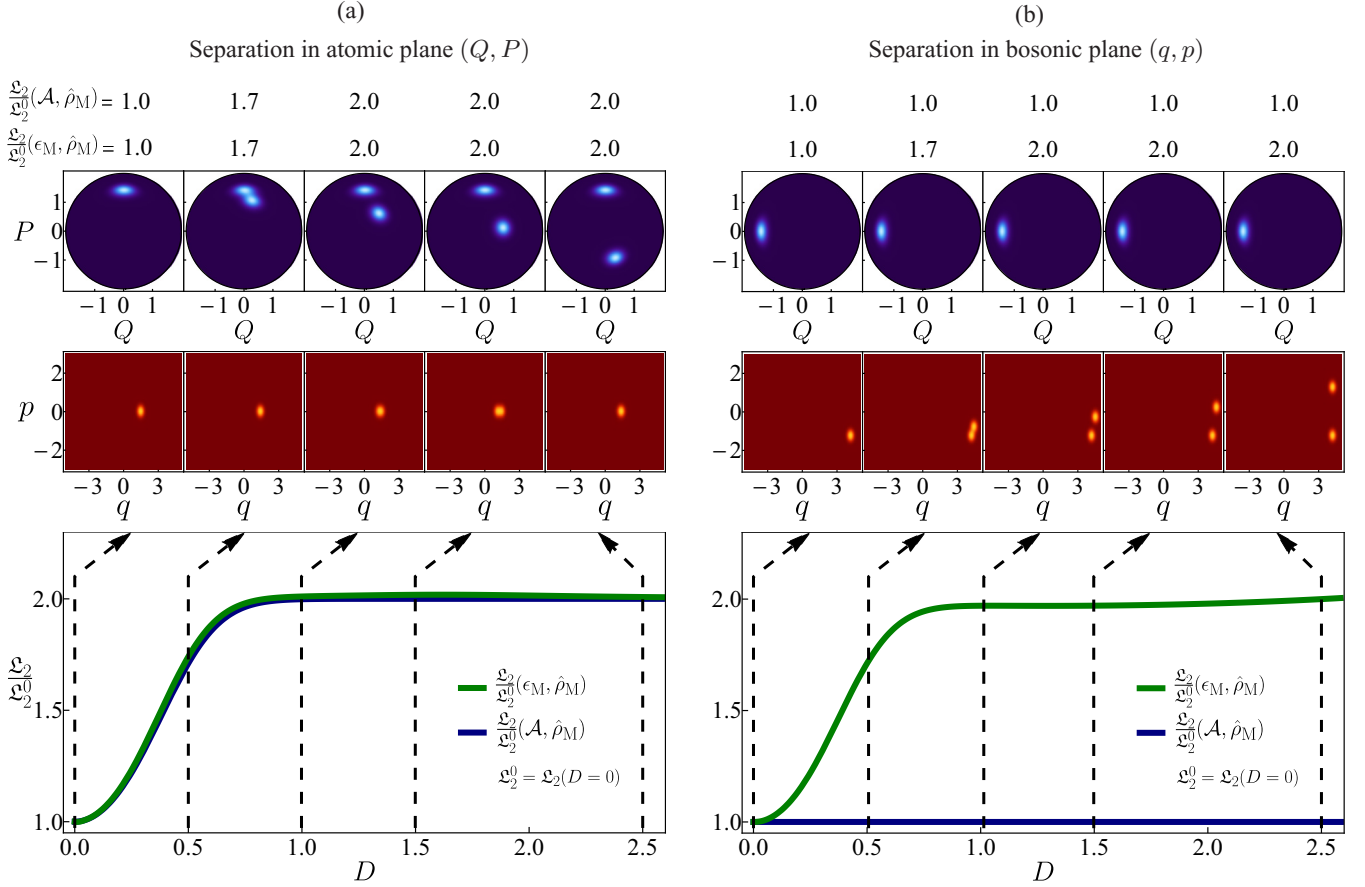


FIG. 4. The top square panels show the Husimi function projected in the atomic ( $Q, P$ ) (blue circles) and bosonic ( $q, p$ ) (red squares) coordinate planes at different phase-space separations  $D$ . Separation is shown in (a) the atomic plane ( $Q, P$ ) and (b) the bosonic plane ( $q, p$ ). The bottom rectangular panels show the Rényi occupations  $\mathcal{L}_2(\mathcal{A}, \hat{\rho}_M)/\mathcal{L}_2^0$  (solid blue curve) and  $\mathcal{L}_2(\epsilon_M, \hat{\rho}_M)/\mathcal{L}_2^0$  (solid green curve) rescaled to their initial values  $\mathcal{L}_2^0 = \mathcal{L}_2(D=0)$  [see Eqs. (24) and (31)] as a function of the phase-space separation  $D$ , for mixed coherent states  $\hat{\rho}_M(D)$  [see Eq. (34)] with constant energy width (a)  $\sigma = 0.429$  and (b)  $\sigma = 0.342$  (units of  $\epsilon$ ) in the chaotic-energy region  $\epsilon_M = 1$ . Vertical dashed black lines indicate the value of  $D$  where the Husimi projections are shown. The system size is  $j = 30$ .

horizontal tubular shapes which cover the available bosonic space only partially.

These results confirm that the Husimi projection over the atomic subspace used in the Rényi occupation  $\mathcal{L}_2(\mathcal{A}, \hat{\rho}_M)$  loses possible localization of the states in the bosonic plane, which is not the case for the Rényi occupation  $\mathcal{L}_2(\epsilon_M, \hat{\rho}_M)$ , which is sensitive to the localization of the states in both planes. In summary, for states well localized in energy, such as the eigenstates and coherent states considered here,  $\mathcal{L}_2(\epsilon, \hat{\rho})$  is a more sensitive measure. However, for states that are delocalized in energy,  $\mathcal{L}_2(\epsilon, \hat{\rho})$  could lose important information about the localization of the states in energy and  $\mathcal{L}_2(\mathcal{A}, \hat{\rho})$  may be more adequate.

## VI. CONCLUSION

In this paper we have put forward a general mathematical framework to define occupation (and from it localization) of quantum states with respect to a given discrete or continuous measure space. Since the measures obtained are related to the Rényi entropies of order  $\alpha \geq 0$ , we called them Rényi occupations of order  $\alpha$ . We showed that this mathematical

framework includes two recently employed localization measures in phase space, used to gauge localization of eigenstates and coherent states in the chaotic region of the Dicke model. One of them measures localization of the Husimi function projected into the atomic phase space, whereas the other measures the localization of the Husimi function over the energy shells of the corresponding classical model.

Both Rényi occupations were compared in detail and the origin of their differences was elucidated. It was shown that the occupation over the atomic subspace can miss information about the localization of states in the bosonic plane. For states well localized in energy, such as eigenstates and coherent states, the occupation over classical energy shells is a more suitable measure of localization in phase space.

We emphasize, however, that there is no unique way to define localization in phase space. In this article, we have focused on the Rényi occupations of order  $\alpha = 2$ , but orders  $\alpha \neq 2$  can be used to reveal other aspects of the Husimi distribution either in classical energy shells or in its projection in the atomic subspace. In general, Rényi occupations with  $\alpha > 1$  strengthen the contribution of regions with largest dis-



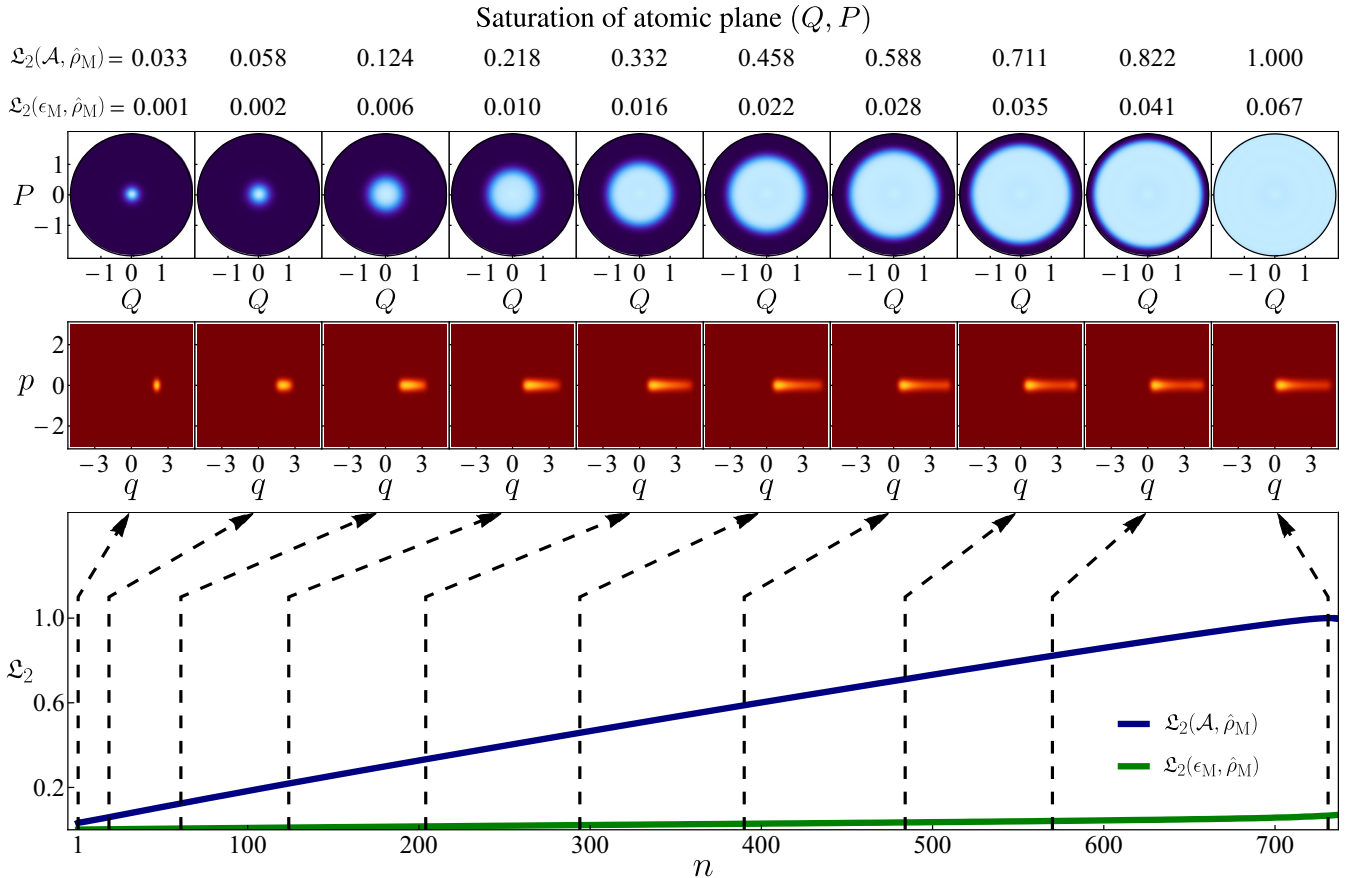


FIG. 5. The top square panels show the Husimi function projected in the atomic ( $Q, P$ ) (blue circles) and bosonic ( $q, p$ ) (red squares) coordinate planes for different numbers of added states  $n$ . The bottom rectangular panel shows Rényi occupations  $\mathcal{L}_2(\mathcal{A}, \hat{\rho}_M)$  (solid blue curve) and  $\mathcal{L}_2(\epsilon_M, \hat{\rho}_M)$  (solid green curve) [see Eqs. (24) and (31)] as a function of the number of added states  $n$ , for mixed coherent states  $\hat{\rho}_M(n)$  [see Eq. (37)] which saturate the atomic plane ( $Q, P$ ) in the chaotic-energy region  $\epsilon_M = 1$ . Vertical dashed black lines indicate the values of  $n$  where the Husimi projections are shown. The system size is  $j = 30$ .

tribution values to the detriment of those with smaller ones; conversely, Rényi occupations of order  $\alpha < 1$  tend to equally weight the contributions of the regions where the probability distribution is different from zero, independently of its value. A study of the dependence of the Rényi occupations on  $\alpha$  would reveal multifractality in the occupation of the states in phase space.

Another interesting issue to be explored in the future is the relationship between the phase-space localization of nonstationary states, as revealed by the Rényi occupations introduced here, and the breaking of the eigenstate thermalization hypothesis (ETH) [77,78]. It is conjectured that a necessary condition for the ETH to be valid is that the infinite-time average of generic nonstationary states reaches an energy-shell Rényi occupation equal to 1. How the localization measure can help identify states that violate the ETH is an open question to be explored in future works.

**ACKNOWLEDGMENTS**

We thank Lea F. Santos for her insightful comments. We acknowledge support from the Computation Center, ICN, in particular Enrique Palacios, Luciano Díaz, and Eduardo Murrieta. D.V., S.P.-C., and J.G.H. acknowledge financial

support from the DGAPA UNAM Project No. IN104020 and S.L.-H. from the Mexican CONACyT Project No. CB2015-01/255702.

**APPENDIX A: DERIVATION OF THE RÉNYI VOLUME**

As in Sec. II, we consider a space  $X$  with a measure  $\mathcal{V}$ , which generates a (Lebesgue) integral  $\int_X d\mathcal{V}(\mathbf{x})$ . We will construct the Rényi volume  $\mathcal{V}_\alpha(X, \varphi)$  given by Eqs. (4) and (3) by requiring the function  $\mathcal{V}(X, \varphi)$  to be equal to  $\mathcal{V}(\Omega)$  for a uniform distribution over  $\Omega \subseteq X$ , to be bounded by the volume of  $X$ , and to be homogeneous under the scaling of  $\mathcal{V}$ .

The easiest function that satisfies these properties is  $\mathcal{V}_0(X, \varphi) = \mathcal{V}(\text{supp}(\varphi))$ , where  $\text{supp}(\varphi) = \{\mathbf{x} \in X \mid \varphi(\mathbf{x}) \neq 0\}$  [which is the limit  $\alpha \rightarrow 0$  of Eq. (3)]. However, this may not be very useful, because  $\varphi$  may be very small (but not zero) in some region of  $X$ . We would want  $\mathcal{V}(X, \varphi)$  to be able to ignore those low-probability regions.

The threshold for when to consider a probability ignorable is of course arbitrary. Let us consider any function  $f : (0, \infty) \rightarrow \mathbb{R}$  so that the value  $f(x)$  establishes how much we care about the regions where  $\varphi(x)$  is less than  $x$ . Then it is

natural to define the weighted mean

$$F(\varphi) = \int_X d\mathcal{V}(\mathbf{x})\varphi(\mathbf{x})f(\varphi(\mathbf{x})). \quad (\text{A1})$$

For a bounded measurable subset  $\Omega \subseteq X$ , we define the uniform probability distribution  $\varphi_\Omega(\mathbf{x})$  as in Eq. (1). For these uniform probabilities, we require  $\mathcal{V}_f(X, \varphi_\Omega) = \mathcal{V}(\Omega)$ . This condition will allow us to find  $\mathcal{V}_f(X, \varphi)$  for any normalized distribution  $\varphi$ .

We have

$$F(\varphi_\Omega) = \int_\Omega d\mathcal{V}(\mathbf{x})\varphi_\Omega(\mathbf{x})f(\varphi_\Omega(\mathbf{x})) = f\left(\frac{1}{\mathcal{V}_f(X, \varphi_\Omega)}\right). \quad (\text{A2})$$

If we require  $f$  to be invertible, then  $\mathcal{V}_f(X, \varphi_\Omega) = 1/f^{-1}(F(\varphi_\Omega))$ . Thus, it is natural to extend this formula and define

$$\mathcal{V}_f(X, \varphi) = \frac{1}{f^{-1}(F(\varphi))} = \left[ f^{-1}\left( \int_X d\mathcal{V}(\mathbf{x})\varphi(\mathbf{x})f(\varphi(\mathbf{x})) \right) \right]^{-1} \quad (\text{A3})$$

for any distribution  $\varphi$ . Note that because  $f^{-1} > 0$ , we have  $\mathcal{V}_f(X, \varphi) > 0$ . However, without imposing some extra conditions on  $f$ , we cannot say anything about the upper bound of  $\mathcal{V}_f(X, \varphi)$ .

Because we wish to interpret  $\mathcal{V}_f(X, \varphi)$  as the volume of the region occupied by  $\varphi$ , we need to first ensure that  $\mathcal{V}_f(X, \varphi) \leq \mathcal{V}(X)$  when  $X$  is bounded. To guarantee this, we require that (a)  $f(x)$  is strictly increasing and  $g(x) = xf(x)$  is convex. Then, by Jensen's inequality (cf. [79]), the convexity of  $g(x) = xf(x)$  guarantees that

$$\begin{aligned} F(\varphi) &= \int_X d\mathcal{V}(\mathbf{x})g(\varphi(\mathbf{x})) \\ &\geq \mathcal{V}(X)g\left(\frac{1}{\mathcal{V}(X)}\int_X d\mathcal{V}(\mathbf{x})\varphi(\mathbf{x})\right) = f\left(\frac{1}{\mathcal{V}(X)}\right) \end{aligned} \quad (\text{A4})$$

for any distribution  $\varphi$  with  $\int_X d\mathcal{V}(\mathbf{x})\varphi(\mathbf{x}) = 1$ . Because  $f^{-1}$  is increasing if  $f$  is increasing, we get

$$\begin{aligned} \mathcal{V}_f(X, \varphi) &= \frac{1}{f^{-1}(F(\varphi))} \leq \frac{1}{f^{-1}(f(1/\mathcal{V}(X)))} = \mathcal{V}(X) \\ &= \mathcal{V}_f(X, \varphi_X), \end{aligned} \quad (\text{A5})$$

where  $\varphi_X$  is the uniform distribution on  $X$ . Note that the argument above also works if (b)  $f(x)$  is strictly decreasing and  $g(x) = xf(x)$  is concave by replacing  $f \rightarrow -f$ . Moreover, Jensen's inequality in Eq. (A4) becomes an equality if and only if there exist  $a, b \in \mathbb{R}$  such that  $xf(x) = g(x) = a + bx$  for all  $x \in \{\varphi(\mathbf{x}) \mid \mathbf{x} \in X\}$  (i.e.,  $g$  is linear in the range of  $\varphi$ ). If either of the stricter conditions, that is, (a')  $f(x)$  is strictly increasing and  $g(x) = xf(x)$  is strictly convex or (b')  $f(x)$  is strictly decreasing and  $g(x) = xf(x)$  is strictly concave, is satisfied, then  $g$  cannot be linear in  $\{\varphi(\mathbf{x}) \mid \mathbf{x} \in X\}$  unless that set consists of a single point, in which case  $\varphi$  must be constant. So either of conditions (a') or (b') implies that  $\mathcal{V}_f(X, \varphi) = \mathcal{V}(X)$  occurs only when  $\varphi = \varphi_X$  is the uniform distribution.

If  $f_1(x) = \ln(x)$ , condition (a') is satisfied and we obtain Eq. (4). For  $f_\alpha(x) = x^{\alpha-1}$  with  $\alpha \geq 0$  and  $\alpha \neq 1$ , condition (a') is satisfied if  $\alpha > 1$ , condition (b') is satisfied if  $0 < \alpha <$

1, and condition (b) [but not condition (b')] is satisfied if  $\alpha = 0$ . In any case, Eq. (A3) yields Eq. (3).

There are many other functions  $f$  besides  $f_1(x) = \ln(x)$  and  $f_\alpha(x) = x^{\alpha-1}$  ( $\alpha > 0$ ,  $\alpha \neq 1$ ) that satisfy condition (a') or (b'). However, the measures  $\mathcal{V}_\alpha(X, \varphi) = \mathcal{V}_{f_\alpha}(X, \varphi)$  given by Eqs. (3) and (4) are the only ones that are homogeneous under scaling of the measure  $\mathcal{V}$  [see Eq. (2)]. If  $\mathcal{V}_f(X, \varphi)$  satisfies Eq. (2), it can be shown that  $f = af_\alpha + b$ , where  $a, b \in \mathbb{R}$  with  $a \neq 0$  [see Theorem (5.2.19) and Eq. (5.2.26) of Ref. [80]]. It is straightforward to verify that  $f' = af + b$  implies  $\mathcal{V}_{f'}(X, \varphi) = \mathcal{V}_f(X, \varphi)$  directly from Eq. (A3). In fact, the converse is also true [see Theorem (5.2.16) of Ref. [80]]. Thus, if  $\mathcal{V}_f(X, \varphi)$  satisfies Eq. (2), then  $\mathcal{V}_f(X, \varphi) = \mathcal{V}_\alpha(X, \varphi)$  for some  $\alpha \geq 0$ .

## APPENDIX B: DIAGONALIZATION BASIS

### 1. Fock basis

The standard Fock basis is given by the tensor product  $|n\rangle \otimes |j, m_z\rangle$ , where  $|n\rangle$  ( $n = 0, 1, 2, \dots$ ) are the eigenstates of the number operator  $\hat{n} = \hat{a}^\dagger \hat{a}$  of the infinite-dimensional bosonic subspace and  $|j, m_z\rangle$  ( $m_z = -j, -j+1, \dots, j-1, j$ ) are the eigenstates of the collective pseudospin operator  $\hat{J}_z$  of the finite-dimensional pseudospin subspace with Hilbert-space dimension  $2j+1$ . As the bosonic subspace has infinite Hilbert-space dimension, we need to truncate it by choosing a maximal excitation level  $n_{\max}$ , which enables us to define a finite dimension  $n_{\max} + 1$ . Then the global Hilbert-space dimension is given by  $\mathcal{D}_{\text{FB}} = (n_{\max} + 1) \times (2j + 1)$ .

For the system size  $j = 30$  selected in this work, we required  $n_{\max} = 420$  with global dimension  $\mathcal{D}_{\text{FB}} = 25\,681$  to ensure  $\mathcal{D}_{\text{FB}}^c = 8030$  converged eigenstates and eigenvalues. For the selected Hamiltonian parameters, the energy spectrum ranges from the ground-state energy  $\epsilon_{\text{GS}} = -2.125$  up to a truncated converged energy  $\epsilon_{\text{T}} = 3.683$ .

An advantage of using the Fock basis is that one may compute exact projections of the Husimi function of a state  $\hat{\rho}$  in both atomic and bosonic subspaces of the Dicke model by using the closed expressions [37,60]

$$\begin{aligned} \tilde{Q}_{\hat{\rho}}(Q, P) &= \frac{j}{2\pi} \iint dq dp Q_{\hat{\rho}}(q, p; Q, P) \\ &= A(Q, P) \sum_{n=0}^{n_{\max}} \sum_{m_z=-j}^j \sum_{m'_z=-j}^j \{ (c_{n, m_z}^{\hat{\rho}})^* c_{n, m'_z}^{\hat{\rho}} \} \\ &\quad \times G_{m_z}^A(Q, P) [G_{m'_z}^A(Q, P)]^*, \end{aligned} \quad (\text{B1})$$

with  $A(Q, P) = \left(1 - \frac{Q^2 + P^2}{4}\right)^{2j}$ , and

$$G_{m_z}^A(Q, P) = \sqrt{\binom{2j}{j+m_z}} \left( \frac{Q + iP}{\sqrt{4 - Q^2 - P^2}} \right)^{j+m_z} \quad (\text{B2})$$

for the atomic projection and

$$\begin{aligned} \tilde{Q}_{\hat{\rho}}(q, p) &= \frac{2j+1}{4\pi} \iint dQ dP Q_{\hat{\rho}}(q, p; Q, P) \\ &= B(q, p) \sum_{n=0}^{n_{\max}} \sum_{n'=0}^{n_{\max}} \sum_{m_z=-j}^j \{ (c_{n, m_z}^{\hat{\rho}})^* c_{n', m_z}^{\hat{\rho}} \} \\ &\quad \times G_n^B(q, p) [G_{n'}^B(q, p)]^*, \end{aligned} \quad (\text{B3})$$

with  $B(q, p) = \exp[-\frac{j}{2}(q^2 + p^2)]$ , and

$$C_n^B(q, p) = \frac{1}{\sqrt{n!}} \left( \sqrt{\frac{j}{2}} (q + ip) \right)^n \quad (\text{B4})$$

for the bosonic one. In both expressions,  $c_{n,m_x}^{\hat{\rho}}$  are the coefficients of the state  $\hat{\rho}$  expanded in this basis.

## 2. Efficient basis

The efficient basis is obtained by taking the eigenbasis of the Dicke Hamiltonian  $\hat{H}_D$  [see Eq. (8)] in the limit  $\omega_0 \rightarrow 0$ . The first step to construct this basis is to define a displaced annihilation operator  $\hat{A} = \hat{a} + [2\gamma/(\omega\sqrt{N})]\hat{J}_x$ . Then a rotation in the Bloch sphere  $(\hat{J}_x, \hat{J}_y, \hat{J}_z) \rightarrow (\hat{J}'_z, \hat{J}'_y, -\hat{J}'_x)$  is performed. Finally, taking the limit  $\omega_0 \rightarrow 0$ , one obtains a basis given by the tensor product  $|N\rangle \otimes |j, m_x\rangle$ , where the states are explicitly

$$|N\rangle \otimes |j, m_x\rangle = \frac{(\hat{A}^\dagger)^N}{\sqrt{N!}} |N=0\rangle \otimes |j, m_x\rangle, \quad (\text{B5})$$

with  $|N\rangle$  the eigenstates of the operator  $\hat{A}^\dagger \hat{A}$  and  $|N=0\rangle \otimes |j, m_x\rangle$  the vacuum state of the modified bosonic subspace which defines coherent states  $|N=0\rangle = |-\gamma m_x/(\omega\sqrt{N})\rangle$  in the standard Fock basis for each value of  $m_x$ , which corresponds to the rotated eigenvalue of the original collective pseudospin operator  $\hat{J}_x$ .

The states of the pseudospin subspace are defined in the same way as in the Fock basis  $|j, m_x\rangle$  ( $m_x = -j, -j+1, \dots, j-1, j$ ) with Hilbert-space dimension  $2j+1$ . As in the Fock basis, there are infinitely many states corresponding to the modified bosonic subspace  $|N\rangle$  ( $N = 0, 1, 2, \dots$ ), so a truncation is also necessary. By choosing a maximal excitation level  $N_{\max}$ , we determine a finite dimension  $N_{\max} + 1$  so that the global Hilbert-space dimension for this basis is given by  $\mathcal{D}_{\text{EB}} = (N_{\max} + 1) \times (2j + 1)$ .

For the selected system size  $j = 30$ , we require  $N_{\max} = 200$  with global dimension  $\mathcal{D}_{\text{EB}} = 12\,261$  to ensure  $\mathcal{D}_{\text{EB}}^c = 8041$  converged eigenstates and eigenvalues. For these Hamiltonian parameters, the energy spectrum ranges from the ground-state energy  $\epsilon_{\text{GS}} = -2.125$  up to a truncated converged energy  $\epsilon_{\text{T}} = 3.688$ .

Although not used in this work, it is worth noting that the efficient basis allows us to reach larger system sizes ( $j \sim 100$ )

in the superradiant phase of the model, which would be unreachable by using the standard Fock basis [61,62,81].

## APPENDIX C: LOWER BOUND ON PHASE-SPACE LOCALIZATION

The Lieb conjecture [82,83] guarantees that the coherent states  $\hat{\rho}_x = |\mathbf{x}\rangle\langle\mathbf{x}|$  are the most localized in the phase space of the Dicke model. Thus,  $\mathcal{V}_\alpha(\mathcal{M}, \hat{\rho}_x)$  is a lower bound on the Rényi volume in phase space for any state. We will define this value as given by Eqs. (3) and (4). Because all coherent states are translations of each other and  $\mathcal{V}$  is invariant under translations in  $\mathcal{M}$  ( $\mathcal{V}$  is the Haar measure for the group of translations of  $\mathcal{M}$ ), it suffices to calculate  $\mathcal{V}_\alpha(\mathcal{M}, \hat{\rho}_c)$  for one coherent state  $\hat{\rho}_c = |\mathbf{c}\rangle\langle\mathbf{c}|$  centered at  $\mathbf{c} \in \mathcal{M}$ . For convenience, let us choose  $\mathbf{c} = (0, 0, 0, 0)$ , so  $|\mathbf{c}\rangle = |q = p = Q = P = 0\rangle$ . The Husimi function of  $|\mathbf{c}\rangle$  is given by [44,84]

$$\mathcal{Q}_c(\mathbf{x}) = \exp\left(-\frac{j}{2}(q^2 + p^2)\right) \left(1 - \frac{P^2 + Q^2}{4}\right)^{2j}. \quad (\text{C1})$$

Inserting Eq. (C1) into Eq. (3) and performing the integration, we get

$$\begin{aligned} \mathcal{V}_\alpha(\mathcal{M}, \hat{\rho}_c) &= 8\pi^2 \hbar_{\text{eff}}^2 (\hbar_{\text{eff}} + 2)^{\alpha/(1-\alpha)} [\alpha(2\alpha + \hbar_{\text{eff}})]^{1/(\alpha-1)} \\ &= (2\pi \hbar_{\text{eff}})^2 \alpha^{2/(\alpha-1)} + O(\hbar_{\text{eff}}^3), \end{aligned} \quad (\text{C2})$$

where  $\hbar_{\text{eff}} = 1/j$ . Using  $\lim_{\alpha \rightarrow 1} \alpha^{2/(\alpha-1)} = e^2$ , we get  $\mathcal{V}_1(\mathcal{M}, \hat{\rho}_c) = (2\pi \hbar_{\text{eff}} e)^2 + O(\hbar_{\text{eff}}^3)$ , which can also be verified by directly integrating Eq. (4),

$$\begin{aligned} \mathcal{V}_1(\mathcal{M}, \hat{\rho}_c) &= \frac{(2\pi \hbar_{\text{eff}})^2 e^{(\hbar_{\text{eff}}+4)/(\hbar_{\text{eff}}+2)}}{\hbar_{\text{eff}} + 2} \\ &= (2\pi \hbar_{\text{eff}} e)^2 + O(\hbar_{\text{eff}}^3). \end{aligned} \quad (\text{C3})$$

The higher-order terms  $O(\hbar_{\text{eff}}^3)$  are small provided that  $\alpha \gg \hbar_{\text{eff}}^2$ , in which case Eq. (16) is valid. If  $\alpha$  is of the order of  $\hbar_{\text{eff}}^2$  or smaller, this is not true anymore. In fact, in the limit of  $\alpha \rightarrow 0$ ,

$$\mathcal{V}_0(\mathcal{M}, \hat{\rho}_c) = \mathcal{V}(\{\mathbf{x} \in \mathcal{M} \mid \mathcal{Q}_c(\mathbf{x}) \neq 0\}) = \mathcal{V}(\mathcal{M}) = \infty. \quad (\text{C4})$$

This happens because, as  $\alpha$  becomes smaller, the Rényi volume  $\mathcal{V}_\alpha(\mathcal{M}, \hat{\rho})$  loses the ability to differentiate between the regions where  $\mathcal{Q}_\hat{\rho}$  is big and the regions where it is small but nonzero. Thus, the Rényi volumes in phase space  $\mathcal{V}_\alpha(\mathcal{M}, \hat{\rho})$  are more useful when  $\alpha \gg \hbar_{\text{eff}}^2$ .

- 
- [1] B. V. Chirikov, F. M. Izrailev, and D. L. Shepelyansky, Dynamical stochasticity in classical and quantum mechanics, *Sov. Sci. Rev. C* **2**, 209 (1981).
- [2] F. M. Izrailev, Simple models of quantum chaos: Spectrum and eigenfunctions, *Phys. Rep.* **196**, 299 (1990).
- [3] G. Casati, B. V. Chirikov, and D. L. Shepelyansky, Quantum Limitations for Chaotic Excitation of the Hydrogen Atom in a Monochromatic Field, *Phys. Rev. Lett.* **53**, 2525 (1984).
- [4] G. Casati, B. V. Chirikov, D. L. Shepelyansky, and I. Guarneri, Relevance of classical chaos in quantum mechanics: The hydrogen atom in a monochromatic field, *Phys. Rep.* **154**, 77 (1987).
- [5] R. Blümel and U. Smilansky, Localization of Floquet States in the rf Excitation of Rydberg Atoms, *Phys. Rev. Lett.* **58**, 2531 (1987).
- [6] P. W. Anderson, Absence of diffusion in certain random lattices, *Phys. Rev.* **109**, 1492 (1958).
- [7] S. Fishman, D. R. Grempel, and R. E. Prange, Chaos, Quantum Recurrences, and Anderson Localization, *Phys. Rev. Lett.* **49**, 509 (1982).
- [8] G. Casati, B. V. Chirikov, I. Guarneri, and F. M. Izrailev, Band-random-matrix model for quantum localization in conservative systems, *Phys. Rev. E* **48**, R1613 (1993).

- [9] F. Borgonovi, G. Casati, and B. Li, Diffusion and Localization in Chaotic Billiards, *Phys. Rev. Lett.* **77**, 4744 (1996).
- [10] B. Batistić and M. Robnik, Semiempirical theory of level spacing distribution beyond the Berry-Robnik regime: Modeling the localization and the tunneling effects, *J. Phys. A: Math. Theor.* **43**, 215101 (2010).
- [11] B. Batistić and M. Robnik, Dynamical localization of chaotic eigenstates in the mixed-type systems: Spectral statistics in a billiard system after separation of regular and chaotic eigenstates, *J. Phys. A: Math. Theor.* **46**, 315102 (2013).
- [12] B. Batistić and M. Robnik, Quantum localization of chaotic eigenstates and the level spacing distribution, *Phys. Rev. E* **88**, 052913 (2013).
- [13] B. Batistić, Č. Lozej, and M. Robnik, Statistical properties of the localization measure of chaotic eigenstates and the spectral statistics in a mixed-type billiard, *Phys. Rev. E* **100**, 062208 (2019).
- [14] M. Robnik, in *Synergetics*, edited by A. Hutt and H. Haken (Springer, New York, 2020), pp. 133–148.
- [15] E. B. Rozenbaum and V. Galitski, Dynamical localization of coupled relativistic kicked rotors, *Phys. Rev. B* **95**, 064303 (2017).
- [16] M. Fava, R. Fazio, and A. Russomanno, Many-body dynamical localization in the kicked Bose-Hubbard chain, *Phys. Rev. B* **101**, 064302 (2020).
- [17] C. Rylands, E. B. Rozenbaum, V. Galitski, and R. Konik, Many-Body Dynamical Localization in a Kicked Lieb-Liniger Gas, *Phys. Rev. Lett.* **124**, 155302 (2020).
- [18] L. L. Campbell, Exponential entropy as a measure of extent of a distribution, *Z. Wahrscheinlichkeitstheor. Gebiete* **5**, 217 (1966).
- [19] L. Jost, Entropy and diversity, *Oikos* **113**, 363 (2006).
- [20] F. Jelinek, R. L. Mercer, L. R. Bahl, and J. K. Baker, Perplexity—A measure of the difficulty of speech recognition tasks, *J. Acoust. Soc. Am.* **62**, S63 (1977).
- [21] P. F. Brown, V. J. D. Pietra, R. L. Mercer, S. A. D. Pietra, and J. C. Lai, An estimate of an upper bound for the entropy of English, *Comput. Ling.* **18**, 31 (1992).
- [22] T. Gorin, H. J. Korsch, and B. Mirbach, Phase-space localization and level spacing distributions for a driven rotor with mixed regular/chaotic dynamics, *Chem. Phys.* **217**, 145 (1997).
- [23] K. Husimi, Some formal properties of the density matrix, *Proc. Phys.-Math. Soc. Jpn.* **22**, 264 (1940).
- [24] A. Wehrl, General properties of entropy, *Rev. Mod. Phys.* **50**, 221 (1978).
- [25] S. Gnutzmann and K. Zyczkowski, Rényi-Wehrl entropies as measures of localization in phase space, *J. Phys. A: Math. Gen.* **34**, 10123 (2001).
- [26] Q. Wang and M. Robnik, Statistical properties of the localization measure of chaotic eigenstates in the Dicke model, *Phys. Rev. E* **102**, 032212 (2020).
- [27] S. Pilatowsky-Cameo, D. Villaseñor, M. A. Bastarrachea-Magnani, S. Lerma-Hernández, L. F. Santos, and J. G. Hirsch, Ubiquitous quantum scarring does not prevent ergodicity, *Nat. Commun.* **12**, 852 (2021).
- [28] R. H. Dicke, Coherence in spontaneous radiation processes, *Phys. Rev.* **93**, 99 (1954).
- [29] K. Hepp and E. H. Lieb, On the superradiant phase transition for molecules in a quantized radiation field: The Dicke maser model, *Ann. Phys. (NY)* **76**, 360 (1973).
- [30] Y. K. Wang and F. T. Hioe, Phase transition in the Dicke model of superradiance, *Phys. Rev. A* **7**, 831 (1973).
- [31] B. M. Garraway, The Dicke model in quantum optics: Dicke model revisited, *Philos. Trans. R. Soc. A* **369**, 1137 (2011).
- [32] P. Kirton, M. M. Roses, J. Keeling, and E. G. Dalla Torre, Introduction to the Dicke model: From equilibrium to nonequilibrium, and vice versa, *Adv. Quantum Technol.* **2**, 1800043 (2019).
- [33] J. Chávez-Carlos, B. López-del-Carpio, M. A. Bastarrachea-Magnani, P. Stránský, S. Lerma-Hernández, L. F. Santos, and J. G. Hirsch, Quantum and Classical Lyapunov Exponents in Atom-Field Interaction Systems, *Phys. Rev. Lett.* **122**, 024101 (2019).
- [34] R. J. Lewis-Swan, A. Safavi-Naini, J. J. Bollinger, and A. M. Rey, Unifying, thermalization and entanglement through measurement of fidelity out-of-time-order correlators in the Dicke model, *Nat. Commun.* **10**, 1581 (2019).
- [35] S. Pilatowsky-Cameo, J. Chávez-Carlos, M. A. Bastarrachea-Magnani, P. Stránský, S. Lerma-Hernández, L. F. Santos, and J. G. Hirsch, Positive quantum Lyapunov exponents in experimental systems with a regular classical limit, *Phys. Rev. E* **101**, 010202(R) (2020).
- [36] M. A. M. de Aguiar, K. Furuya, C. H. Lewenkopf, and M. C. Nemes, Chaos in a spin-boson system: Classical analysis, *Ann. Phys. (NY)* **216**, 291 (1992).
- [37] K. Furuya, M. A. M. de Aguiar, C. H. Lewenkopf, and M. C. Nemes, Husimi distributions of a spin-boson system and the signatures of its classical dynamics, *Ann. Phys. (NY)* **216**, 313 (1992).
- [38] L. Bakemeier, A. Alvermann, and H. Fehske, Dynamics of the Dicke model close to the classical limit, *Phys. Rev. A* **88**, 043835 (2013).
- [39] S. Pilatowsky-Cameo, D. Villaseñor, M. A. Bastarrachea-Magnani, S. Lerma-Hernández, L. F. Santos, and J. G. Hirsch, Quantum scarring in a spin-boson system: Fundamental families of periodic orbits, *New J. Phys.* **23**, 033045 (2021).
- [40] A. Altland and F. Haake, Equilibration and macroscopic quantum fluctuations in the Dicke model, *New J. Phys.* **14**, 073011 (2012).
- [41] M. Kloc, P. Stránský, and P. Cejnar, Quantum quench dynamics in Dicke superradiance models, *Phys. Rev. A* **98**, 013836 (2018).
- [42] S. Lerma-Hernández, J. Chávez-Carlos, M. A. Bastarrachea-Magnani, L. F. Santos, and J. G. Hirsch, Analytical description of the survival probability of coherent states in regular regimes, *J. Phys. A: Math. Theor.* **51**, 475302 (2018).
- [43] S. Lerma-Hernández, D. Villaseñor, M. A. Bastarrachea-Magnani, E. J. Torres-Herrera, L. F. Santos, and J. G. Hirsch, Dynamical signatures of quantum chaos and relaxation time scales in a spin-boson system, *Phys. Rev. E* **100**, 012218 (2019).
- [44] D. Villaseñor, S. Pilatowsky-Cameo, M. A. Bastarrachea-Magnani, S. Lerma, L. F. Santos, and J. G. Hirsch, Quantum vs classical dynamics in a spin-boson system: Manifestations of spectral correlations and scarring, *New J. Phys.* **22**, 063036 (2020).
- [45] T. Jaako, Z.-L. Xiang, J. J. Garcia-Ripoll, and P. Rabl, Ultrastrong-coupling phenomena beyond the Dicke model, *Phys. Rev. A* **94**, 033850 (2016).

- [46] M. P. Baden, K. J. Arnold, A. L. Grimsmo, S. Parkins, and M. D. Barrett, Realization of the Dicke Model Using Cavity-Assisted Raman Transitions, *Phys. Rev. Lett.* **113**, 020408 (2014).
- [47] Z. Zhang, C. H. Lee, R. Kumar, K. J. Arnold, S. J. Masson, A. L. Grimsmo, A. S. Parkins, and M. D. Barrett, Dicke-model simulation via cavity-assisted Raman transitions, *Phys. Rev. A* **97**, 043858 (2018).
- [48] J. Cohn, A. Safavi-Naini, R. J. Lewis-Swan, J. G. Bohnet, M. Gärtner, K. A. Gilmore, J. E. Jordan, A. M. Rey, J. J. Bollinger, and J. K. Freericks, Bang-bang shortcut to adiabaticity in the Dicke model as realized in a Penning trap experiment, *New J. Phys.* **20**, 055013 (2018).
- [49] A. Safavi-Naini, R. J. Lewis-Swan, J. G. Bohnet, M. Gärtner, K. A. Gilmore, J. E. Jordan, J. Cohn, J. K. Freericks, A. M. Rey, and J. J. Bollinger, Verification of a Many-Ion Simulator of the Dicke Model through Slow Quenches Across a Phase Transition, *Phys. Rev. Lett.* **121**, 040503 (2018).
- [50] M. J. W. Hall, Universal geometric approach to uncertainty, entropy, and information, *Phys. Rev. A* **59**, 2602 (1999).
- [51] E. Ott, *Chaos in Dynamical Systems* (Cambridge University Press, Cambridge, 2002).
- [52] N. C. Murphy, R. Wortis, and W. A. Atkinson, Generalized inverse participation ratio as a possible measure of localization for interacting systems, *Phys. Rev. B* **83**, 184206 (2011).
- [53] A. Rényi, in *Proceedings of the Fourth Berkeley Symposium on Mathematical Statistics and Probability, Volume 1: Contributions to the Theory of Statistics* (University of California Press, Berkeley, 1961), pp. 547–561.
- [54] C. E. Shannon, A mathematical theory of communication, *Bell Syst. Tech. J.* **27**, 379 (1948).
- [55] D. Nath, Properties of Rényi complexity ratio of quantum-states: An extension of generalized Rényi complexity, [arXiv:2008.05418](https://arxiv.org/abs/2008.05418).
- [56] M. A. Bastarrachea-Magnani, B. López-del-Carpio, J. Chávez-Carlos, S. Lerma-Hernández, and J. G. Hirsch, Delocalization and quantum chaos in atom-field systems, *Phys. Rev. E* **93**, 022215 (2016).
- [57] K. Hepp and E. H. Lieb, Equilibrium statistical mechanics of matter interacting with the quantized radiation field, *Phys. Rev. A* **8**, 2517 (1973).
- [58] C. Emary and T. Brandes, Chaos and the quantum phase transition in the Dicke model, *Phys. Rev. E* **67**, 066203 (2003).
- [59] J. Chávez-Carlos, M. A. Bastarrachea-Magnani, S. Lerma-Hernández, and J. G. Hirsch, Classical chaos in atom-field systems, *Phys. Rev. E* **94**, 022209 (2016).
- [60] M. A. M. de Aguiar, K. Furuya, C. H. Lewenkopf, and M. C. Nemes, Particle-spin coupling in a chaotic system: Localization-delocalization in the Husimi distributions, *Europhys. Lett.* **15**, 125 (1991).
- [61] M. A. Bastarrachea-Magnani, S. Lerma-Hernández, and J. G. Hirsch, Comparative quantum and semiclassical analysis of atom-field systems. I. Density of states and excited-state quantum phase transitions, *Phys. Rev. A* **89**, 032101 (2014).
- [62] M. A. Bastarrachea-Magnani, S. Lerma-Hernández, and J. G. Hirsch, Comparative quantum and semiclassical analysis of atom-field systems. II. Chaos and regularity, *Phys. Rev. A* **89**, 032102 (2014).
- [63] M. A. Bastarrachea-Magnani, B. López del Carpio, S. Lerma-Hernández, and J. G. Hirsch, Chaos in the Dicke model: Quantum and semiclassical analysis, *Phys. Scr.* **90**, 068015 (2015).
- [64] A. D. Ribeiro, M. A. M. de Aguiar, and A. F. R. de Toledo Piza, The semiclassical coherent state propagator for systems with spin, *J. Phys. A: Math. Gen.* **39**, 3085 (2006).
- [65] M. Hillery, R. F. O’Connell, M. O. Scully, and E. P. Wigner, Distribution functions in physics: Fundamentals, *Phys. Rep.* **106**, 121 (1984).
- [66] E. Wigner, On the quantum correction for thermodynamic equilibrium, *Phys. Rev.* **40**, 749 (1932).
- [67] A. Z. Goldberg, A. B. Klimov, M. Grassl, G. Leuchs, and L. L. Sánchez-Soto, Extremal quantum states, *AVS Quantum Sci.* **2**, 044701 (2020).
- [68] M. C. Gutzwiller, Periodic orbits and classical quantization conditions, *J. Math. Phys.* **12**, 343 (1971).
- [69] M. C. Gutzwiller, *Chaos in Classical and Quantum Mechanics* (Springer, New York, 1990).
- [70] M. Schreiber and H. Grussbach, Multifractal Wave Functions at the Anderson Transition, *Phys. Rev. Lett.* **67**, 607 (1991).
- [71] A. D. Mirlin and F. Evers, Multifractality and critical fluctuations at the Anderson transition, *Phys. Rev. B* **62**, 7920 (2000).
- [72] A. D. Mirlin, Statistics of energy levels and eigenfunctions in disordered systems, *Phys. Rep.* **326**, 259 (2000).
- [73] F. Evers and A. D. Mirlin, Anderson transitions, *Rev. Mod. Phys.* **80**, 1355 (2008).
- [74] A. Rodriguez, L. J. Vasquez, K. Slevin, and R. A. Römer, Critical Parameters from a Generalized Multifractal Analysis at the Anderson Transition, *Phys. Rev. Lett.* **105**, 046403 (2010).
- [75] J. Martin, I. García-Mata, O. Giraud, and B. Georgeot, Multifractal wave functions of simple quantum maps, *Phys. Rev. E* **82**, 046206 (2010).
- [76] R. Dubertrand, I. García-Mata, B. Georgeot, O. Giraud, G. Lemarié, and J. Martin, Multifractality of quantum wave functions in the presence of perturbations, *Phys. Rev. E* **92**, 032914 (2015).
- [77] R. Nandkishore and D. A. Huse, Many-body localization and thermalization in quantum statistical mechanics, *Annu. Rev. Condens. Matter Phys.* **6**, 15 (2015).
- [78] D. A. Abanin, E. Altman, I. Bloch, and M. Serbyn, Colloquium: Many-body localization, thermalization, and entanglement, *Rev. Mod. Phys.* **91**, 021001 (2019).
- [79] R. Durrett, *Probability: Theory and Examples*, 5th ed. (Cambridge University Press, Cambridge, 2019), p. 21.
- [80] J. Aczél and Z. Daróczy, in *On Measures of Information and their Characterizations*, edited by J. Aczél and Z. Daróczy (Elsevier, Amsterdam, 1975), Vol. 115, Chap. 5, pp. 134–172.
- [81] Q.-H. Chen, Y.-Y. Zhang, T. Liu, and K.-L. Wang, Numerically exact solution to the finite-size Dicke model, *Phys. Rev. A* **78**, 051801(R) (2008).
- [82] E. H. Lieb, Proof of an entropy conjecture of Wehrl, *Commun. Math. Phys.* **62**, 35 (1978).
- [83] E. H. Lieb and J. P. Solovej, Proof of an entropy conjecture for Bloch coherent spin states and its generalizations, *Act. Math.* **212**, 379 (2014).
- [84] F. T. Arecchi, E. Courtens, R. Gilmore, and H. Thomas, Atomic coherent states in quantum optics, *Phys. Rev. A* **6**, 2211 (1972).